PHYSICAL REVIEW E **104**, 034204 (2021)

Signal amplification enhanced by large phase disorder in coupled bistable units

Xiaoming Liang [1,*] and Xiyun Zhang [2,†]

[1] *School of Physics and Electronic Engineering, Jiangsu Normal University, Xuzhou 221116, China*
[2] *Department of Physics, Jinan University, Guangzhou, Guangdong 510632, China*

(Received 27 April 2021; revised 23 August 2021; accepted 23 August 2021; published 7 September 2021)

We study the maximum response of network-coupled bistable units to subthreshold signals focusing on the effect of phase disorder. We find that for signals with large levels of phase disorder, the network exhibits an enhanced response for intermediate coupling strength, while generating a damped response for low levels of phase disorder. We observe that the large phase-disorder-enhanced response depends mainly on the signal intensity but not on the signal frequency or the network topology. We show that a zero average activity of the units caused by large phase disorder plays a key role in the enhancement of the maximum response. With a detailed analysis, we demonstrate that large phase disorder can suppress the synchronization of the units, leading to the observed resonancelike response. Finally, we examine the robustness of this phenomenon to the unit bistability, the initial phase distribution, and various signal waveform. Our result demonstrates a potential benefit of phase disorder on signal amplification in complex systems.

DOI: 10.1103/PhysRevE.104.034204

I. INTRODUCTION

Traditionally, the noise accompanying a desired signal is regarded as a disadvantageous factor in signal processing. However, under some circumstances, noise can become helpful for the detection of a faint signal [1–3], and this constructive role is known as stochastic resonance [4,5]. Because of its generic nature, stochastic resonance has been observed in various nonlinear systems, including ring lasers, nanomechanical oscillators, sensory receptors, and climate networks [6–10]. In most scenarios, noise comes from environmental variability [11], whereas it may also arise from the intrinsic diversity of the individual units composing the systems [12–14]. For instance, no two neurons are identical, even when they are from the same neural network and are of the same type [15,16]. Unlike environmental noise varying with time, the intrinsic diversity is almost time-independent; however, it can play a constructive role in signal amplification similar to that of noise. This effect is termed diversity-induced resonance [17–19]. Moreover, heterogeneous network topology such as irregular structures and weighted connections provide another source of diversity that may enhance the amplification of faint signals [20–24].

Most studies in signal amplification focused on the case of identical initial phases, i.e., the signal phases reaching the units are the same. This setting of identical initial phases might not fit the realistic scenarios, since phase difference in the arriving signals provides a major cue for sensory neurons to locate the signal source [25,26]. For instance, the owl tracks the sound source by comparing the interaural phase difference between two ears [27,28]; the clawed frog measures the direction by detecting the time differences along the lateral-line organs [29,30]. Therefore, to better understand the mechanism underlying signal detection in biological systems, it is essential to investigate the role of phase difference.

To this end, Brandt *et al.* studied the dynamics of coupled chaotic pendula driven by disordered forces. With increasing the level of phase disorder of the driven forces, the motion pattern of coupled pendula changes from chaotic to regular [31,32]. Later on, Liang *et al.* investigated the response of globally coupled excitable neurons to subthreshold signals with phase disorder. Compared to identical phases, an optimal level of disordered phases can induce coherent neuronal firing activity [33]. Recently, Chacón *et al.* explored the impact of phase disorder on the maximum response of coupled overdamped bistable units, and found that the resonantlike amplifying effect of scale-free network structure is drastically reduced when the level of phase disorder in external signals is increased [34].

In this paper, we investigate how phase disorder can affect the maximum response of network-coupled bistable units to subthreshold signals, and find that phase disorder can assist in signal amplification under certain circumstances. We show that this desired effect appears only for large levels of phase disorder and intermediate values of coupling strength. We further show that this effect is sensitive to the signal intensity, while it is insensitive to the signal frequency and the network topology. Utilizing reduced models, we reveal the mechanism underlying the positive effect of large phase disorder in signal amplification. Finally, we discuss the applicability of this mechanism in more complex situations. Our findings, on the one hand, complement the study of Ref. [34]; on the other hand, they can help us understand the dual role of phase disorder in signal processing.

II. MODEL

We consider a network of overdamped, periodically forced bistable units. The dynamics of a single unit is given by

$$\dot{x} = x - x^3 + A\sin(\omega t + \phi). \tag{1}$$

*xmliang@jsnu.edu.cn
†xiyunzhang@jnu.edu.cn

In the absence of periodic forcing ($A = 0$), Eq. (1) has two nonzero solutions:

$$x(t) = \pm\left[1 - \left(1 - x_0^{-2}\right)e^{-2t}\right]^{-\frac{1}{2}}, \tag{2}$$

with $x_0 = x(0)$. As $t \to \infty$, $x(t)$ approaches the stable fixed points $x_s = \pm 1$. When a subthreshold signal is introduced, i.e., $A < A_c$, the unit vibrates around one of the two stable fixed points, whereas for $A \geqslant A_c$, it can switch between them. Accordingly, A_c is a threshold intensity which tends to $A_c = 2\sqrt{3}/9$ for long signal period $T = 2\pi/\omega$ [19,35].

The dynamics of N coupled overdamped bistable units are given as follows:

$$\dot{x}_i = x_i - x_i^3 + \lambda \sum_{j=1}^{N} L_{ij}(x_j - x_i) + A\sin(\omega t + \phi_i), \tag{3}$$

with $i = 1, \cdots, N$. λ is the coupling strength, and L_{ij} is the element of the adjacency matrix L representing the structure of the network. Specifically, $L_{ij} = L_{ji} = 1$ if units i and j are connected, and zero otherwise. Note that Eq. (3) is a paradigmatic model for studying signal amplification and propagation in complex systems under the influence of noise [35–40]. Here, we use it to study the effect of phase disorder on signal amplification. If not specified otherwise, then the initial phase ϕ_i follows a uniform distribution on the interval $[-\gamma\pi, \gamma\pi)$, where $\gamma \in [0, 1]$ controls the level of phase disorder.

As all units are subjected to external signals with the same period, it is convenient to characterize their dynamics by the amplitudes

$$g_i = \frac{\max_t x_i - \min_t x_i}{2} \tag{4}$$

and the centers

$$c_i = \frac{\max_t x_i + \min_t x_i}{2}. \tag{5}$$

According to Eq. (4), the maximum response of the network to external signals is given by [20,34]

$$G = \max_{i=1}^{N} g_i. \tag{6}$$

To reveal the connection between the maximum response and the network synchronization, we apply the degree of spatial synchronization of the units as [20,41]

$$\rho = \frac{|n_+ - n_-|}{N}, \tag{7}$$

where n_+ and n_- are the number of units in the positive ($c_i > \theta$) and negative ($c_i < -\theta$) well, respectively. θ is a threshold, fixed to $\theta = 0.2$, which is applied to determine the states of the units. If half of the units vibrate in the positive well and the other half in the negative well, i.e., $n_+ = n_- = N/2$, then the network is asynchronous with $\rho = 0$. On the contrary, if all units vibrate in the same well, i.e., $n_+ = N$ or $n_- = N$, then the network is synchronous with $\rho = 1$. Note that if all units oscillate widely between the wells, i.e., $-\theta \leqslant c_i \leqslant \theta$, then $n_+ = n_- = 0$ and the degree of spatial synchronization is also $\rho = 0$.

Regarding the numerical simulations, the initial conditions of the units are randomly chosen from the two fixed points $x_s = \pm 1$, the maximum response and the degree of spatial synchronization are obtained by averaging results from 500 independent realizations over different initial conditions.

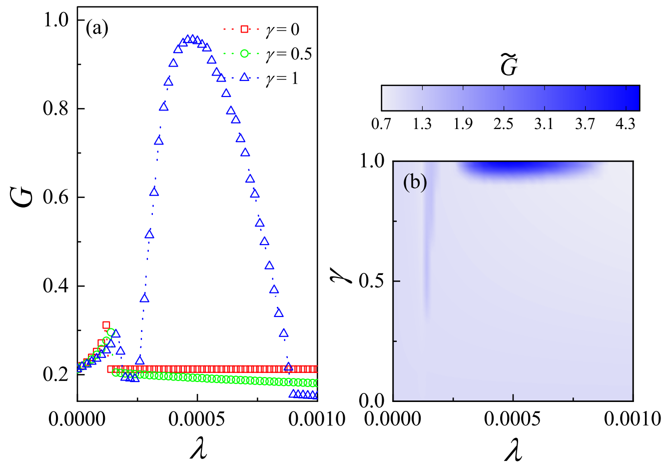

FIG. 1. (a) The maximum response G of Eq. (3) versus coupling strength λ for $\gamma = 0$, 0.5, 1. (b) The normalized maximum response $\widetilde{G} = G(\gamma)/G(0)$ versus coupling strength λ and level of phase disorder γ.

III. NUMERICAL RESULTS

A. Signal amplification in a global network

Let us first consider the case of a global network with $L_{ij} = 1$, $\forall\, i \neq j$, driven by subthreshold signals with intensity $A = 0.35$ and period $T = 100$ [the intensity threshold is $A_c \approx 0.41$ at this period, see Fig. 3(a)]. Figure 1 plots the maximum response G as a function of coupling strength λ for three different levels of phase disorder γ. In the absence of phase disorder ($\gamma = 0$), the maximum response G increases with λ until a critical coupling strength $\lambda_c = 1.2 \times 10^{-4}$, after which it drops down to the value as at $\lambda = 0$. For an intermediate level of phase disorder (e.g., $\gamma = 0.5$), the maximum response G attains the peak at $\lambda_c = 1.4 \times 10^{-4}$, and then decreases linearly with λ, exhibiting a smaller value than that of $\gamma = 0$. In contrast, for sufficiently large phase disorder ($\gamma = 1$), the critical coupling strength is slightly increased to $\lambda_c = 1.6 \times 10^{-4}$, but the value of G is largely enhanced from $\lambda_1 = 2.6 \times 10^{-4}$ to $\lambda_2 = 9 \times 10^{-4}$ with a secondary peak at $\lambda = 5 \times 10^{-4}$, which is much higher than the first one at λ_c. To obtain an overall view, we show in Fig. 1(b) the dependence of $\widetilde{G}$ on the combination of λ and γ, where $\widetilde{G} = G(\gamma)/G(0)$ is the normalized maximum response divided by the value in the absence of phase disorder. The enhanced response $\widetilde{G}$ (i.e., $\widetilde{G} > 1$) appears only for large levels of phase disorder $\gamma \approx 1$ combined with intermediate values of coupling strength $\lambda \in (\lambda_1, \lambda_2)$. These results demonstrate that phase disorder in subthreshold signals does not always weaken signal amplification, but can also enhance it under certain circumstances.

In Fig. 2(a) we show the degree of spatial synchronization ρ corresponding to the maximum response G as depicted in Fig. 1(a). A sharp transition is observed from $\rho \approx 0$ to $\rho = 1$ at the critical coupling strength λ_c. Beyond λ_c, the degree of spatial synchronization ρ remains unchanged for

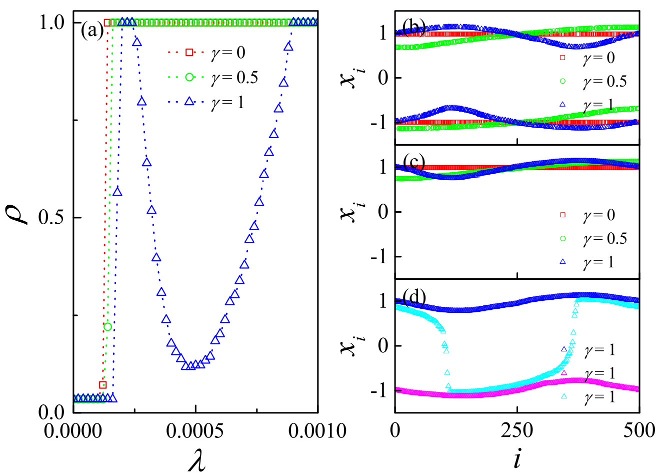

FIG. 2. (a) The degree of spatial synchronization ρ of Eq. (3) versus coupling strength λ for $\gamma = 0, 0.5, 1$. Snapshots of the spatial positions of the units are shown in panel (b) for $\lambda = 5 \times 10^{-5}$, in panel (c) for $\lambda = 2 \times 10^{-4}$, and in panel (d) for $\lambda = 5 \times 10^{-4}$, where the indices of the units are rearranged based on the rank of the initial phases of driven signals.

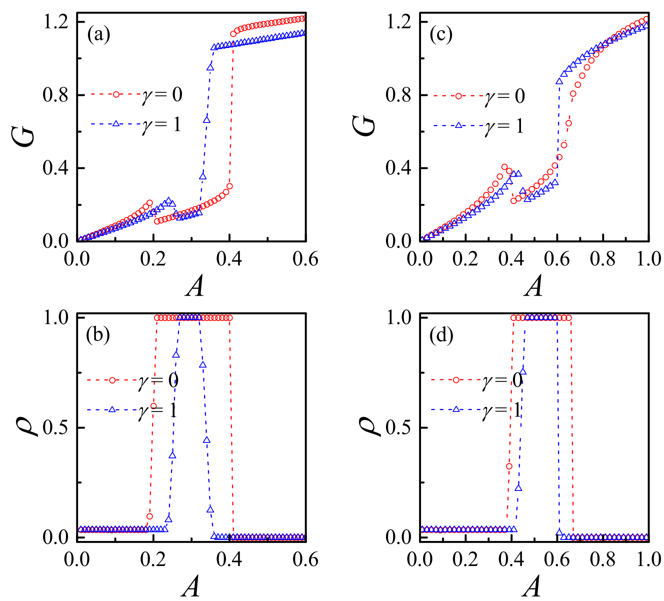

FIG. 3. The maximum response G and the degree of spatial synchronization ρ versus signal intensity A for $\gamma = 0$ and $\gamma = 1$. The period of external signals is $T = 100$ for panels (a, b) and $T = 10$ for panels (c, d). The coupling strength $\lambda = 5 \times 10^{-4}$ is used in Eq. (3).

$\gamma = 0$ and $\gamma = 0.5$, while it decreases to $0 < \rho < 1$ on the interval (λ_1, λ_2) for $\gamma = 1$. To illustrate the details of these different transitions, Figs. 2(b)–2(d) show the snapshots for spatial positions of the units, where the indices of the units are rearranged based on the rank of the initial phases of driven signals. The spatial position x_i exhibits relevance to the initial phase ϕ_i approximately satisfying $x_i \approx c_i + g_i \sin(\phi_i)$. In addition, x_i distributes differently for different coupling strength. When $\lambda \leqslant \lambda_c$, the units are randomly distributed into the two wells, according to their initial conditions [see Fig. 2(b)]. This gives $n_+ \approx n_- \approx N/2$ that corresponds to the situation of network desynchronization with $\rho \approx 0$. When $\lambda > \lambda_c$, the units are synchronized at the same well, resulting in $n_+ = N$, $n_- = 0$, and $\rho = 1$ for $\gamma = 0$ and $\gamma = 0.5$, respectively [see Fig. 2(c)]. However, for $\gamma = 1$ the spatial positions of the units display three different stationary states on the interval (λ_1, λ_2): (i) concentrates at the positive well (network synchronization with $\rho = 1$), (ii) concentrates at the negative well (network synchronization with $\rho = 1$), and (iii) distributes across the two wells (network desynchronization with $\rho \approx 0$) [see Fig. 2(d)]. Further, when the coupling strength is too large, i.e., $\lambda > \lambda_2$, the desynchronous state across two wells vanishes, only two synchronous states concentrating at the positive or negative well remain. Comparing the maximum response during these possible stationary states, we find that the enhanced signal amplification occurs only for the desynchronous state. Therefore, the network desynchronization induced by large phase disorder accounts for the resonancelike behavior observed in Fig. 1.

In Fig. 3 we investigate the effect of signal intensity on the maximum response. When the global network is subjected to identical signals with a long period $T = 100$, the maximum response G first increases for small A, then slightly drops at $A_1 = 0.19$, and finally jumps discontinuously at the intensity threshold $A_c \approx 0.41$ [see Fig. 3(a)]. Figure 3(b) shows the degree of spatial synchronization ρ corresponding to Fig. 3(a). It can be seen that the slight drop of G is associated with a synchronization transition from $\rho \approx 0$ to $\rho = 1$, indicating that the units are driven to vibrate at the same well. In comparison, the discontinuous jump of G is due to the dynamics of the units changes from an intrawell vibration to an interwell oscillation, manifested by the degree of spatial synchronization changes from $\rho = 1$ to $\rho = 1$. When the large phase disorder ($\gamma = 1$) is present, the value of A_1 is increased to $A_1' = 0.24$, whereas the intensity threshold is decreased to $A_c' = 0.34$. A similar phenomenon can be found for the signals with a short period $T = 10$ [see Fig. 3(c)]. In the case of short-period signals, there is no obvious intensity threshold A_c, since the maximum response G increases continuously when $A > A_1 = 0.38$. However, as shown in Fig. 3(d), the degree of spatial synchronization transits from $\rho = 1$ to $\rho = 0$ at $A = 0.68$, which can be considered as the intensity threshold A_c for the short-period signals. Summarizing the observations in Fig. 3, the amplifying effect of large phase disorder appears for a broad range of signal periods, while it depends strongly on the signal intensity, and is most obvious when the signal intensity closes to the intensity threshold.

B. Signal amplification in complex networks

The amplifying effect of large phase disorder is not specific to the global network structure. In Fig. 4 we compare the maximum response G between identical signals ($\gamma = 0$) and phase-disordered signals ($\gamma = 1$) in small-world (SW) and scale-free (SF) networks, respectively. The SW network is constructed by the Watts-Strogatz algorithm [42] with an average degree $\langle k \rangle = 4$ and a rewiring probability $p = 0.2$. The SF network is constructed by the Barabasi-Albert algorithm [43] with an average degree $\langle k \rangle = 4$. Figure 4 shows the maximum response and the degree of spatial synchronization as a

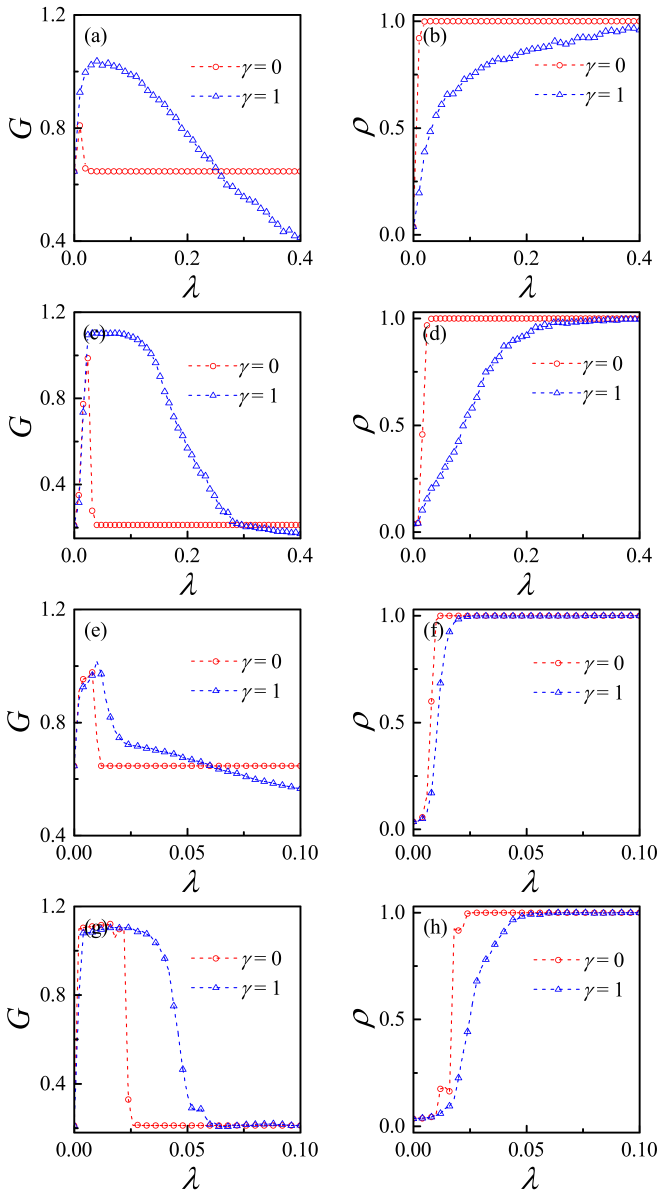

FIG. 4. The maximum response G and the degree of spatial synchronization ρ versus coupling strength λ for $\gamma = 0$ and $\gamma = 1$ in SW and SF networks. (a, b) SW network with $T = 100$ and $A = 0.35$, (c, d) SW network with $T = 10$ and $A = 0.65$, (e, f) SF network with $T = 100$ and $A = 0.35$, and (g, h) SF network with $T = 10$ and $A = 0.65$.

function of coupling strength. For the SW network, the signal can be amplified for a wide range of coupling strength with the presence of large phase disorder, whereas can be amplified only for very small λ when the phase disorder is absent [see Figs. 4(a) and 4(c)]. This enhancement in signal amplification can be ascribed to that large phase disorder can suppress the synchronization among the units [see Figs. 4(b) and 4(d)]. With this suppression, for relatively strong coupling strength some units can still keep oscillating between two wells, leading to the wide range of signal amplification. Similarly, for the SF network large phase disorder in the driven signals can also suppress network synchronization, which results in an amplifying effect for relatively strong coupling strength [see Figs. 4(e)–4(h)]. However, it has been reported that the maximum response drastically reduces with increasing the level of phase disorder in SF networks [34]. The explanation for this is that the signal intensity of the driven signals is set to $A = 0.01$ in Ref. [34] which is far from the intensity threshold, so making a drastic reduction of signal amplification. Our results in Fig. 4 demonstrate that large phase disorder is harmful for network synchronization but is useful for amplification of subthreshold signals.

IV. ANALYSIS

In this section, we propose an underlying mechanism for the large phase-disorder-enhanced signal amplification. For simplicity, we take the global network as an example. Then Eq. (3) becomes

$$\dot{x}_i = (1 - \lambda N)x_i - x_i^3 + \lambda N X + A \sin(\omega t + \phi_i), \qquad (8)$$

where $X = \langle x_i \rangle$ represents the average activity of the units and the angles $\langle \cdot \rangle = N^{-1} \sum_{i=1}^{N}$ denote the ensemble average. In Eq. (8) the average activity drives all units, which plays a crucial role in signal amplification. As seen in Fig. 2, the average activity becomes zero for the intermediate coupling interval (λ_1, λ_2) corresponding to the enhanced maximum response of $\gamma = 1$. To understand the emergence of the zero average activity, we define the potential of Eq. (8) as

$$V_i = (\lambda N - 1)\frac{x_i^2}{2} + \frac{x_i^4}{4} - \lambda N X x_i - x_i A \sin(\omega t + \phi_i). \qquad (9)$$

As the initial conditions of the units are assigned randomly, we can consider a zero average activity $X = 0$ at $t = 0$. With this assumption, we next explore how the zero average activity evolves when the network is subjected to signals without and with phase disorder, respectively. Substituting $X = 0$ into Eq. (9), the potential becomes

$$V_i = (\lambda N - 1)\frac{x_i^2}{2} + \frac{x_i^4}{4} - x_i A \sin(\omega t + \phi_i). \qquad (10)$$

With $\gamma = 0$ at $t = 0$, Eq. (10) describes a symmetrical potential with two wells and one barrier in between [see Fig. 5(a)]. As t evolves to $t = T/4$, the external signal arrives at the maximum which can reduce the potential barrier directionally, namely, Eq. (10) becomes a single-well potential [see Fig. 5(a)]. In this situation, the units initially assigned at the negative well can jump to the positive well. Once all units are at the positive well, they attain fully synchronization behaving like a single unit, i.e., Eq. (3) at $\lambda = 0$. This indicates that the zero average activity originated from random initial conditions cannot be maintained by identical signals on the coupling interval (λ_1, λ_2). With $\gamma = 1$, the initial phases distribute uniformly over the full range $-\pi \leqslant \phi_i < \pi$, which allows two signals with $\phi_i = \pi/2$ and $\phi_i = -\pi/2$ to arrive at the maximum and minimum from the beginning ($t = 0$), respectively. Then one unit initially at the negative well driven by the signal with $\phi_i = -\pi/2$ will jump to the positive well, and another unit initially at the positive well driven by the signal with $\phi_i = \pi/2$ will jump to the negative well [see Figs. 5(b) and 5(c)]. With the evolving of time, there always exists signals satisfying $\omega t + \phi_i = 2j\pi \pm \pi/2$, $j = 1, 2, \cdots$. As a result, units with vanished potential barriers are always

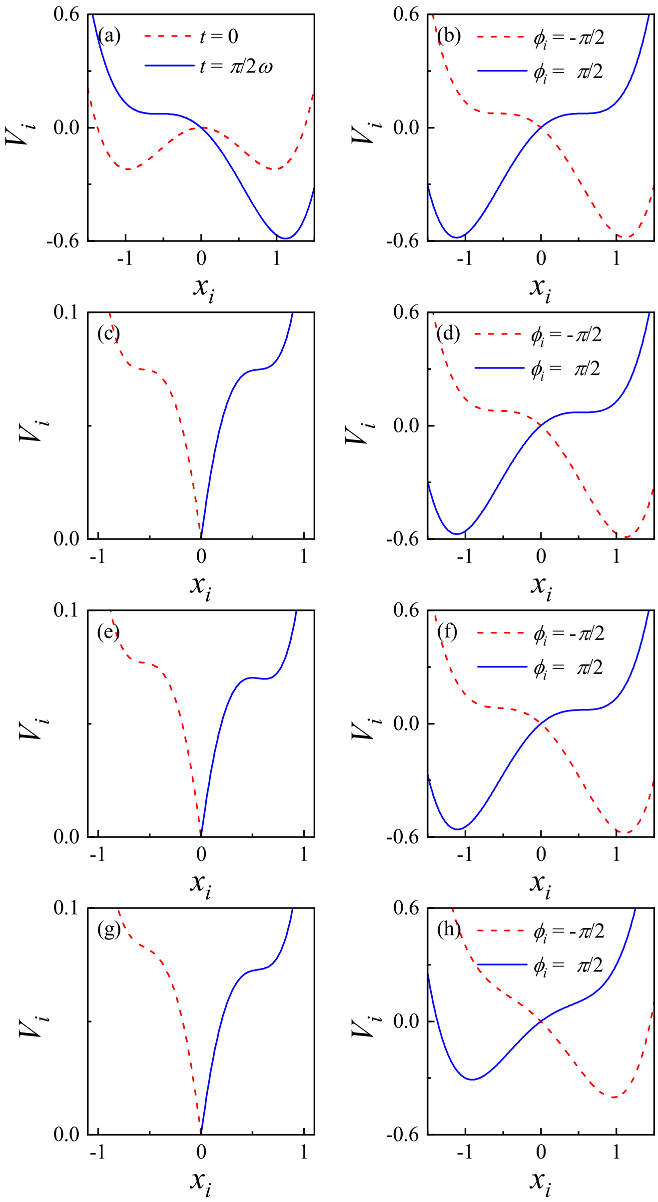

FIG. 5. The potential V_i of Eq. (9) for various combinations of parameters. (a) $\phi_i = 0$, $X = 0$, $\lambda = 1.4 \times 10^{-4}$, (b) $t = 0$, $\phi_i = \pm\pi/2$, $X = 0$, $\lambda = 1.4 \times 10^{-4}$, (d) $t = 0$, $\phi_i = \pm\pi/2$, $X = 0.1$, $\lambda = 1.4 \times 10^{-4}$, (f) $t = 0$, $\phi_i = \pm\pi/2$, $X = 0.1$, $\lambda = 1.8 \times 10^{-4}$, and (h) $t = 0$, $\phi_i = \pm\pi/2$, $X = 0.1$, $\lambda = 1 \times 10^{-3}$. Panels (c, e, g) are the enlarged views of panels (b, d, f), respectively.

existing with time, and the symmetrical jumps across the wells occur sequentially. As a consequence of this process, the zero average activity is maintained for $\gamma = 1$.

The analyses mentioned above are based on the assumption of $X = 0$. However, due to the random initial conditions, the average activity usually deviates from zero, which may affect significantly the symmetry of the potential. For instance, at $t = 0$ a small deviation of $X = 0.1$ can lift (reduce) the potential barrier of Eq. (9) with $\phi_i = -\pi/2$ ($\phi_i = \pi/2$) for the units in the positive (negative) well [see Figs. 5(d) and 5(e)]. This asymmetrical potential leads to a directional preference of jump which, in turn, induces a larger deviation of X, and eventually causes the network synchronization. Under such circumstance, increasing coupling strength can effectively lower the potential barrier, which overcomes the asymmetry induced by $X \neq 0$ [see Figs. 5(f) and 5(g)]. This explains why we observe the amplifying effect of the large phase disorder at a slightly larger coupling λ_1 other than at λ_c. However, if the coupling strength is increased too much, over λ_2, then it changes obviously the symmetry of the potential, which makes one of the two wells deeper and that facilitates the network synchronization [see Fig. 5(h)].

The damped response of the global network for $0 < \gamma < 1$ can be understood in the same manner. The initial phases are distributed in a range narrower than $[-\pi, \pi)$ for $\gamma < 1$. When $t > t_c$, the potential barriers start to disappear directionally, where $t_c = \min(T/4 - \gamma T/2, 0)$. Thus, the units will jump into one well and synchronize within it.

To understand the dependence of the maximum response on the phase disorder, we next derive an analytical relation between them focusing on the global network. Specifically, we only discuss the cases of $\gamma = 0$ and $\gamma = 1$, since the maximum responses are similar when $\gamma < 1$ [see Fig. 1].

A. Case I: $\gamma = 0$

For signals without phase disorder, the network undergoes a synchronization transition from $X \approx 0$ to $X \approx 1$ at λ_c. When $\lambda \leqslant \lambda_c$, we thus assume $X = 0$ in Eq. (8) and obtain

$$\dot{x}_i = (1 - \lambda N)x_i - x_i^3 + A\sin(\omega t + \phi), \tag{11}$$

where the initial phase $\phi_i = \phi$. Using the method of linearization, we can obtain the approximate solution of Eq. (11) as

$$x_i(t) = \pm\sqrt{1 - \lambda N} + \frac{A}{\sqrt{4(1 - \lambda')^2 + \omega^2}}\sin(\omega t + \psi), \tag{12}$$

where ψ is the phase shift. When $\lambda > \lambda_c$, the network attains full synchronization, i.e., $X = x_i$, then Eq. (8) becomes

$$\dot{x}_i = x_i - x_i^3 + A\sin(\omega t). \tag{13}$$

Its approximate solution follows the form of

$$x_i(t) = 1 + \frac{A}{\sqrt{4 + \omega^2}}\sin(\omega t + \psi'), \tag{14}$$

where ψ' represents the phase shift. Combining these results yields

$$G = \begin{cases} \frac{1}{\sqrt{4(1-\lambda N)^2+\omega^2}}, & \text{if } \lambda \leqslant \lambda_c, \\ \frac{1}{\sqrt{4+\omega^2}}, & \text{if } \lambda > \lambda_c. \end{cases} \tag{15}$$

Equation (15) indicates that the maximum response of the global network appears at $\lambda = \lambda_c$, and then drops to a constant. Figure 6(a) shows the estimation of Eq. (15), which exhibits a similar tendency to the result obtained from Eq. (3).

Following [24], we estimate the critical coupling strength for network synchronization shown in Fig. 2(a). It satisfies

$$\left(\frac{A}{2}\right)^2 = \left(\frac{1 - \lambda N}{3}\right)^3. \tag{16}$$

For $A = 0.35$, Eq. (16) gives $\lambda_c = 1.2 \times 10^{-4}$, which is consistent with the result of $\gamma = 0$ shown in Fig. 2(a). When λ is

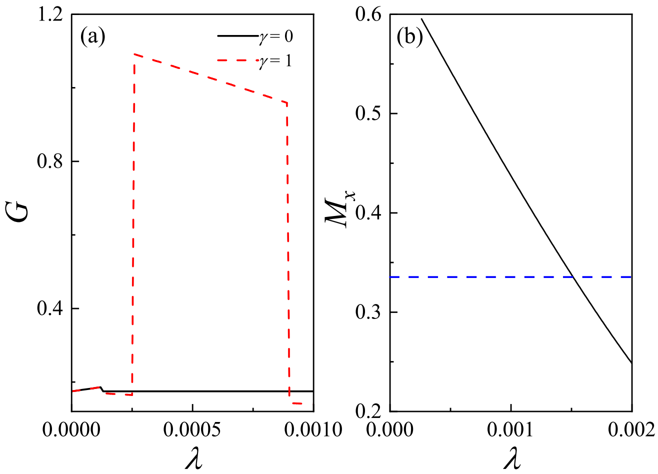

FIG. 6. (a) The analytical maximum response G for $\gamma = 0$ and $\gamma = 1$, obtained from Eqs. (15) and (22) for a global network with $T = 100$ and $A = 0.35$. (b) The analytical M_x of Eq. (25) versus coupling strength λ, where the dashed line denotes $M_x = 1/3$.

just over λ_c, the signals become suprathreshold in Eq. (11), driving all units to the same well and leading to network synchronization. After network synchronization, the coupling term in Eq. (8) vanishes and Eq. (11) becomes Eq. (13).

B. Case II: $\gamma = 1$

For signals with the large phase disorder $\gamma = 1$, both the critical coupling strength λ_c and the average activity X are analogous to those of $\gamma = 0$ when $\lambda \leqslant \lambda_c$ [see Fig. 2]. Thus, we just need to investigate the influence of $X \approx \pm 1$ and $X \approx 0$ on signal amplification for $\lambda > \lambda_c$. In the case of $X \approx \pm 1$, Eq. (8) takes the form

$$\dot{x}_i = (1 - \lambda N)x_i - x_i^3 \pm \lambda N + A\sin(\omega t + \phi_i). \tag{17}$$

According to Eq. (16), the external signal is always subthreshold in Eq. (17). Using the method of linearization, the approximate solution of Eq. (17) is obtained as

$$x_i(t) = \pm 1 + \frac{A}{\sqrt{(2 + \lambda N)^2 + \omega^2}} \sin(\omega t + \psi''), \tag{18}$$

where ψ'' denotes the phase shift. The amplitude of Eq. (18) decreases with λ, indicating a damped response for $X \approx \pm 1$.

In the case of $X \approx 0$, Eq. (8) becomes

$$\dot{x}_i = (1 - \lambda N)x_i - x_i^3 + A\sin(\omega t + \phi_i). \tag{19}$$

From Eq. (16), the external signal becomes suprathreshold in Eq. (19) when $\lambda > \lambda_c$. Thus, the unit can oscillate between the two wells, following the variation of the signal. This is the mechanism underlying the enhanced maximum response for $\gamma = 1$.

Assuming the frequency ω is sufficiently low, the solution of Eq. (19) can be approximately described by the cubic function:

$$(1 - \lambda N)x_i - x_i^3 + A = 0. \tag{20}$$

Solving this function, we obtain

$$x_i(t) = 2\alpha\cosh\left[\frac{1}{3}\text{arcosh}\left(\frac{A}{2\alpha^3}\right)\right]\sin(\omega t + \phi_i), \tag{21}$$

where $\alpha = \sqrt{\frac{1-\lambda N}{3}}$. In summary, the analytical maximum response of the global network for $\gamma = 1$ is obtained as

$$G = \begin{cases} \frac{1}{\sqrt{4(1-\lambda N)^2+\omega^2}}, & \text{if } \lambda \leqslant \lambda_c, \\ \frac{1}{\sqrt{(2+\lambda N)^2+\omega^2}}, & \text{if } \lambda_c < \lambda \leqslant \lambda_1, \\ 2\alpha\cosh\left[\frac{1}{3}\text{arcosh}\left(\frac{A}{2\alpha^3}\right)\right], & \text{if } \lambda_1 < \lambda < \lambda_2, \\ \frac{1}{\sqrt{(2+\lambda N)^2+\omega^2}}, & \text{if } \lambda \geqslant \lambda_2. \end{cases} \tag{22}$$

The prediction of Eq. (22) is shown in Fig. 6(a). The maximum response is enhanced only on the intermediate coupling interval (λ_1, λ_2). However, there exists a disagreement between the analytic prediction and the numerical result [see Figs. 1(a) and 6(a)]. The reason for this disagreement is that, the global network can exhibit both damped and enhanced responses on this coupling interval. The maximum response shown in Fig. 1(a) is the result averaged over these two responses, rather than only the enhanced one.

Finally, we explain why the zero average activity disappears at λ_2. Let $x_i = X + \delta_i$, we average Eq. (8) over the ensemble and achieve

$$\dot{X} = X - X^3 - 3X\langle\delta_i^2\rangle - \langle\delta_i^3\rangle. \tag{23}$$

Considering $X \approx 0$ and using Eq. (21), the trajectory deviation is

$$\delta_i \approx x_i \approx 2\alpha\cosh\left[\frac{1}{3}\text{arcosh}\left(\frac{A}{2\alpha^3}\right)\right]\sin(\omega t + \phi_i). \tag{24}$$

As the initial phases are uniformly distributed between $-\pi$ to π, leading to $\langle\sin(\omega t + \phi_i)\rangle = 0$, $\langle\sin^2(\omega t + \phi_i)\rangle = 1/2$, and $\langle\sin^3(\omega t + \phi_i)\rangle = 0$. Accordingly, the variance

$$M_x = \langle\delta_i^2\rangle \approx 2\alpha^2\cosh^2\left[\frac{1}{3}\text{arcosh}\left(\frac{A}{2\alpha^3}\right)\right] \tag{25}$$

and the odd moment $\langle\delta_i^3\rangle \approx 0$. Then Eq. (23) can be rewritten as

$$\dot{X} = (1 - 3M_x)X - X^3. \tag{26}$$

Equation (26) has three fixed points $X^* = \pm\sqrt{1 - 3M_x}$ and $X^* = 0$, which can be considered as the three stationary states of $X \approx \pm 1$ and $X \approx 0$. The stability of these fixed points is determined by the value of M_x. With the increase of coupling strength till $M_x > 1/3$, the fixed point $X^* = 0$ becomes unstable, while the other two fixed points $X^* = \pm\sqrt{1 - 3M_x}$ become stable. This corresponds to the transition from network desynchronization to synchronization at λ_2. Submitting $M_x = 1/3$ into Eq. (25), we obtain the analytical coupling strength $\lambda_2 = 1.5 \times 10^{-3}$, which is much larger than the numerical result shown in Fig. 1(a). This is due to that the analytical variance M_x of Eq. (25) is obtained from an ideal condition of $X = 0$, and it decreases with λ since λ_1 [see Fig. 6(b)]. However, for simulations with finite size of the network we have $X \neq 0$, and thus the value of M_x is smaller than Eq. (25) as the amplitudes of the units are smaller than Eq. (21). This makes $M_x = 1/3$ happen before $\lambda_2 = 1.5 \times 10^{-3}$, resulting in the deviation between the simulation result and the analytic prediction. Thus, the analytical coupling strength $\lambda_2 = 1.5 \times 10^{-3}$ gives only the upper boundary of the coupling strength for synchronization for the global network with $\gamma = 1$.

Similarly, we can analyze the stability of the states $X \approx \pm 1$. Using Eq. (18), the variance now becomes

$$M_x \approx \frac{A^2}{2(2+\lambda N)^2 + 2\omega^2} \approx 0. \tag{27}$$

Putting it into Eq. (26), we can find that the states $X \approx \pm 1$ are stable for arbitrary coupling strength when $\gamma = 1$.

V. ROBUSTNESS

A. Other examples of bistable systems

To evaluate how robust the above results are to the dynamics of bistable system, we provide two other examples of bistable systems that exhibit the signal amplification enhanced by large phase disorder. We first show a global network of N Duffing oscillators with damping parameter $\delta = 0.25$ [44,45]:

$$\begin{aligned} \dot{x}_i &= y_i, \\ \dot{y}_i &= -\delta y_i + x_i - x_i^3 + \lambda \sum_{j=1}^{N} (x_j - x_i) \\ &\quad + A \sin(\omega t + \phi_i). \end{aligned} \tag{28}$$

Without coupling ($\lambda = 0$), the single Duffing oscillator has a double-well potential with two minima at $x_s = \pm 1$. With a subthreshold periodic forcing, the oscillator vibrates with a small amplitude in one well. With a suprathreshold periodic forcing, the oscillator oscillates with a large amplitude between the two wells. For $T = 100$, the intensity threshold for the transition from intrawell vibration to interwell oscillation is $A_c \approx 0.4$. We calculate from $x_i(t)$ the amplitude g_i of the oscillator according to Eq. (4). Figure 7(a) shows the maximum response of the network to subthreshold signals as a function of coupling strength for identical and disordered phases, respectively. Similarly, the maximum response G is enhanced by large phase disorder at the intermediate coupling strength. Figures 7(b) and 7(c) further show the phase portraits of one representative oscillator at two coupling strength for $\gamma = 1$. When the coupling strength is weak $\lambda = 1 \times 10^{-4}$, the oscillator vibrates in one of the two wells depending on its initial condition. However, as λ is increased to an intermediate value $\lambda = 3 \times 10^{-4}$, the oscillator starts to cross the wells under the effect of phase disorder.

As the next example we consider a global network of N Lorenz oscillators, whose dynamics are described by [46,47]

$$\begin{aligned} \dot{x}_i &= \sigma(y_i - x_i) + \lambda \sum_{j=1}^{N} (x_j - x_i), \\ \dot{y}_i &= r x_i - y_i - x_i z_i + A \sin(\omega t + \phi_i), \\ \dot{z}_i &= x_i y_i - b z_i, \end{aligned} \tag{29}$$

where $\sigma = 10$, $b = 8/3$, $r = 19$, $A = 16$, and $T = 100$. With these parameters, the single Lorenz oscillator ($\lambda = 0$) rotates in the neighborhood of one of two fixed points $C^{\pm} = (\pm\sqrt{b(r-1)}, \pm\sqrt{b(r-1)}, r-1)$, which may be treated as a generalized bistable system. Note that, the single Lorenz oscillator starts to exhibit irregular switches between the fixed points when $A \geqslant A_c \approx 36.06$ at $T = 100$. Similarly, we use $x_i(t)$ to calculate the amplitude g_i of the Lorenz oscillator according to Eq. (4). The results presented in Fig. 8(a) demonstrate the large phase-disorder-enhanced response in coupled Lorenz oscillators. Moreover, Figs. 8(b) and 8(c) present two trajectories of one representative Lorenz oscillator on x-y plane for weak and intermediate coupling strength,

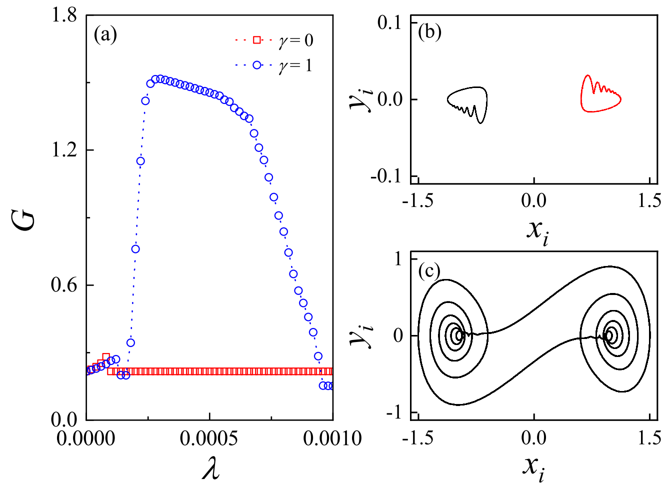

FIG. 7. (a) The maximum response G of Eq. (28) versus coupling strength λ for $\gamma = 0$ and $\gamma = 1$. Phase portraits of one representative oscillator i from Eq. (28) for $\gamma = 1$: (b) two possible intrawell rotations at $\lambda = 1 \times 10^{-4}$ depending on the initial condition of the Duffing oscillator, (c) interwell oscillation at $\lambda = 1 \times 10^{-4}$. The intensity $A = 0.35$ and the period $T = 100$ are used.

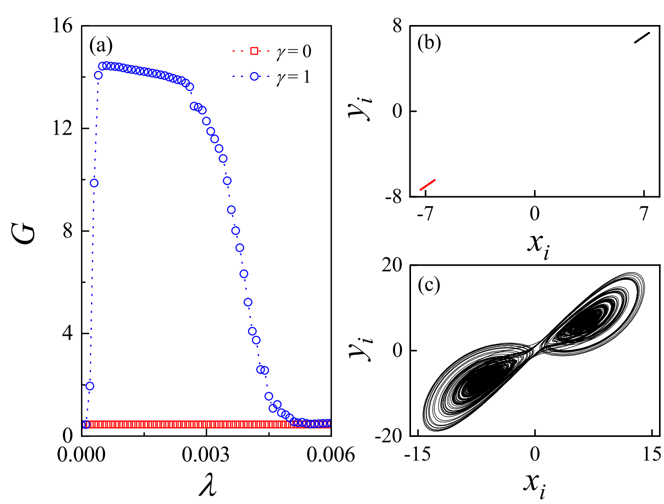

FIG. 8. (a) The maximum response G of Eq. (29) versus coupling strength λ for $\gamma = 0$ and $\gamma = 1$. Phase portraits of one representative oscillator i from Eq. (29) for $\gamma = 1$: (b) two possible limit cycles about one of two fixed points at $\lambda = 5 \times 10^{-5}$ depending on the initial condition of the Lorenz oscillator, (c) irregular switches between two fixed points at $\lambda = 1 \times 10^{-3}$. The intensity $A = 16$ and the period $T = 100$ are used.

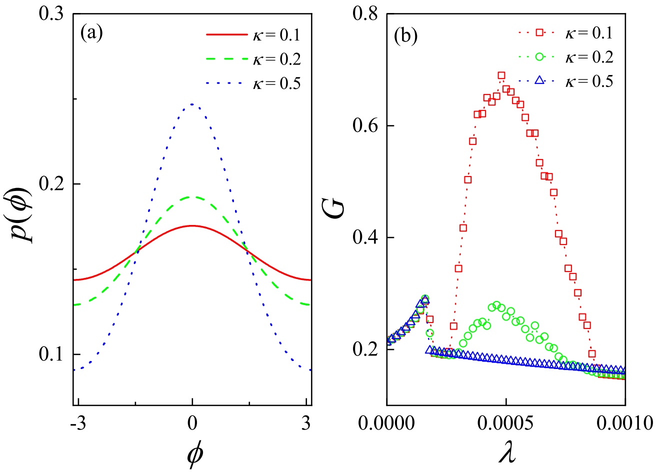

FIG. 9. (a) Density of the von Mises distribution (30) for $\kappa = 0.1, 0.2, 0.5$. (b) The maximum response G of Eq. (3) versus coupling strength λ for $\kappa = 0.1$, 0.2, 0.5. The intensity $A = 0.35$ and the period $T = 100$ are used.

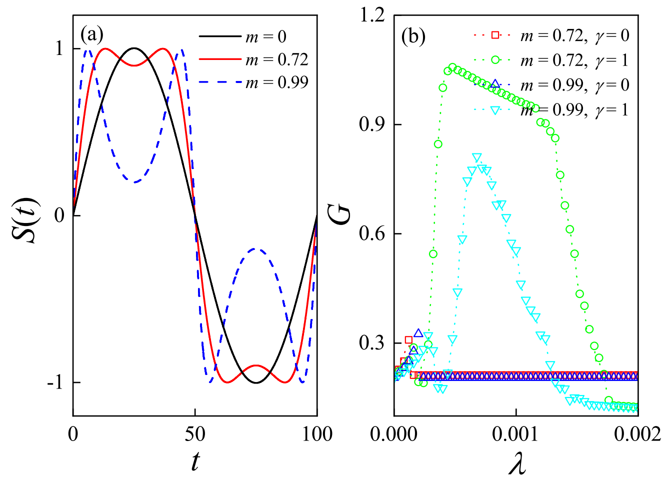

FIG. 10. (a) Signal $S(t)$ of Eq. (31) versus t for $m = 0$, 0.72, 0.99. (b) The maximum response G of Eq. (3) versus coupling strength λ for $m = 0.72$ and $m = 0.99$. The parameters $A = 0.35$ and $T = 100$ are used.

respectively. Likewise, the oscillator transits from a small-amplitude limit cycle to a large-amplitude irregular oscillation with the aid of large phase disorder.

B. Influence of the phase distribution on signal amplification

Next, we investigate how the phase distribution affects signal amplification. To illustrate this, we assume that the initial phases of the subthreshold signals follow the von Mises distribution (also known as the circular normal distribution) with probability density function [48]

$$p(\phi) = \frac{e^{\kappa \cos(\phi)}}{2\pi I_0(\kappa)}, \tag{30}$$

where $\phi \in [-\pi, \pi)$ is the random initial phase, I_0 is the modified Bessel function of the first kind and order zero, and $\kappa \geqslant 0$ is the concentration parameter. Figure 9(a) shows the density for three different κ: 0.1, 0.2, 0.5. For small κ, the distribution tends to the uniform distribution, while approaching a Gaussian distribution for large κ. Fixing $A = 0.35$ and $T = 100$, Fig. 9(b) shows the maximum response G of Eq. (3) as a function of coupling strength, corresponding to the three distributions of phase disorder shown in Fig. 9(a). As κ increases, the amplifying effect of phase disorder gradually weakens and eventually disappears. The reason for the disappearance is that, with high κ the distribution of initial phases is narrow, and most driven signals are nearly identical. These nearly identical signals drive the oscillators in to a highly synchronous state, and thus destroying the zero average activity of the network.

C. Influence of the signal waveform on signal amplification

The discussions above assume that the external signal received by each unit is a sine function. In fact, sine wave is a ideal wave form, and most signals in nature are more complex than this. Signal amplification of complex waveforms has been studied in Refs. [49–53]. We here check the influence of signal waveform on the amplifying effect of the large phase disorder. Following previous efforts [52,53], we now consider that the external signal in Eq. (3) takes the form:

$$S(t) = AN(m)\mathrm{sn}\left[\frac{2K\omega}{\pi}\left(t + \frac{\phi}{\omega}\right)\right]\mathrm{dn}\left[\frac{2K\omega}{\pi}\left(t + \frac{\phi}{\omega}\right)\right], \tag{31}$$

where A is the signal intensity, ϕ is the initial phase, $\mathrm{sn}[\cdot] = \mathrm{sn}[\cdot; m]$ and $\mathrm{dn}[\cdot] = \mathrm{dn}[\cdot; m]$ are Jacobian elliptic functions of parameter $m \in [0, 1]$. $K = K(m)$ is the complete elliptic integral of the first kind. $N(m) = 1/[a + b/(1 + e^{(m-c)/d})]$ is a normalization function with $a = 0.43932$, $b = 0.69796$, $c = 0.3727$, and $d = 0.26883$, which is introduced for the signal to have the same intensity A [52]. Here, the parameter m changes the waveform of the signal Eq. (31) and the illustrations are shown in Fig. 10(a). When $m = 0$, the pulse returns to the sine wave, while becoming narrow for high value of $m \approx 1$. In addition, Fig. 10(b) illustrates the maximum response for $m = 0.72$ and $m = 0.99$ by fixing $A = 0.35$ and $T = 100$. Similarly, the maximum response is enhanced for large phase disorder and intermediate coupling strength, suggesting that the amplifying effect of large phase-disorder-enhanced response can be applied for more complex signals. Note that, the maximum response at the intermediate $m = 0.72$ is higher than that of $m = 0$ and $m = 0.99$, which is because the signal (31) has the largest waveform area at $m = 0.72$ [52].

VI. CONCLUSION

In conclusion, we have studied the maximum response of network-coupled overdamped bistable units to subthreshold signals with disordered phases. When the phases are sufficiently disordered, the network can exhibit a resonancelike response by varying the coupling strength, compared with the damped response of the signals with moderately disordered or fully identical phases. We have shown that the effect of phase-disorder-induced resonance is sensitive to the signal intensity, which becomes evident near the intensity threshold. We also showed that this effect is robust to the signal frequency and the network topology. Taking the global network as an example, we have analyzed the mechanism underlying this phenomenon, and found that large phase disorder can cause network desynchronization with a zero average activity leading to the resonantlike response. We finally demonstrated the robustness of this mechanism, and found that it can be applied for different bistable systems, various phase distributions, and also for signals with more complex waveforms. These results imply that phase disorder has an important impact on signal amplification, and complex systems may benefit from it to regulate their responses to external signals.

ACKNOWLEDGMENTS

X.L. was supported by the NNSF of China under Grants No. 12175087 and No. 61877030. X.Z. was supported by the NNSF of China under Grant No. 12105117, and by the Fundamental Research Funds for the Central Universities (Grant No. 21621007). We thank the anonymous reviewers for critical comments that helped improve the paper.

[1] K. Wiesenfeld and F. Moss, Nature (London) **373**, 33 (1995).
[2] P. Jung and K. Wiesenfeld, Nature (London) **385**, 291 (1997).
[3] J. J. Collins, Nature (London) **402**, 241 (1999).
[4] H. Gang, H. Haken, and X. Fagen, Phys. Rev. Lett. **77**, 1925 (1996).
[5] L. Gammaitoni, P. Hänggi, P. Jung, and F. Marchesoni, Rev. Mod. Phys. **70**, 223 (1998).
[6] L. Gammaitoni, P. Hänggi, P. Jung, and F. Marchesoni, Eur. Phys. J. B **69**, 1 (2009).
[7] K. Kitajo, D. Nozaki, L. M. Ward, and Y. Yamamoto, Phys. Rev. Lett. **90**, 218103 (2003).
[8] A. R. Bulsara, Nature (London) **437**, 962 (2005).
[9] I. Tiwari, J. M. Cruz, P. Parmananda, and M. Rivera, Phys. Rev. E **100**, 060202(R) (2019).
[10] M. Das and H. Kantz, Phys. Rev. E **101**, 062145 (2020).
[11] F. Sagués, J. M. Sancho, and J. García-Ojalvo, Rev. Mod. Phys. **79**, 829 (2007).
[12] C. Zhou, J. Kurths, and B. Hu, Phys. Rev. Lett. **87**, 098101 (2001).
[13] H. Chen and J. Zhang, Phys. Rev. E **77**, 026207 (2008).
[14] M. D. McDonnell and L. M. Ward, Nat. Rev. Neurosci. **12**, 415 (2011).
[15] M. I. Rabinovich, P. Varona, A. I. Selverston, and H. D. I. Abarbanel, Rev. Mod. Phys. **78**, 1213 (2006).
[16] K. Padmanabhan and N. N. Urban, Nat. Neurosci. **13**, 1276 (2010).
[17] C. J. Tessone, C. R. Mirasso, R. Toral, and J. D. Gunton, Phys. Rev. Lett. **97**, 194101 (2006).
[18] L. Wu, S. Zhu, and X. Luo, Chaos **20**, 033113 (2010).
[19] X. Liang, X. Zhang, and L. Zhao, Chaos **30**, 103101 (2020).
[20] J. A. Acebrón, S. Lozano, and A. Arenas, Phys. Rev. Lett. **99**, 128701 (2007).
[21] M. Perc, Phys. Rev. E **78**, 036105 (2008).
[22] T. Kondo, Z. Liu, and T. Munakata, Phys. Rev. E **81**, 041115 (2010).
[23] C. Liu and X. Liang, Phys. Rev. E **100**, 032206 (2019).
[24] X. Liang, C. Liu, and X. Zhang, Phys. Rev. E **101**, 022205 (2020).
[25] B. Grothe, Nat. Rev. Neurosci. **4**, 540 (2003).
[26] J. W. H. Schnupp and C. E. Carr, Nat. Neurosci. **12**, 692 (2009).
[27] M. Konishi, Sci. Am. **16**, 28 (2006).
[28] B. Grothe, Trends Neurosci. **41**, 115 (2018).
[29] Jan-Moritz P. Franosch, M. C. Sobotka, A. Elepfandt, and J. L. van Hemmen, Phys. Rev. Lett. **91**, 158101 (2003).
[30] Jan-Moritz P. Franosch, M. Lingenheil, and J. L. van Hemmen, Phys. Rev. Lett. **95**, 078106 (2005).
[31] S. F. Brandt, B. K. Dellen, and R. Wessel, Phys. Rev. Lett. **96**, 034104 (2006).
[32] P. J. Martínez and R. Chacón, Phys. Rev. Lett. **100**, 144101 (2008).
[33] X. Liang, M. Dhamala, L. Zhao, and Z. Liu, Phys. Rev. E **82**, 010902(R) (2010).
[34] R. Chacón and P. J. Martínez, Phys. Rev. E **92**, 012821 (2015).
[35] R. Chacón, Phys. Rev. E **54**, 6153 (1996).
[36] D. H. Zanette, Phys. Rev. E **55**, 5315 (1997).
[37] Y. Zhang, G. Hu, and L. Gammaitoni, Phys. Rev. E **58**, 2952 (1998).
[38] J. F. Lindner, S. Chandramouli, A. R. Bulsara, M. Löcher, and W. L. Ditto, Phys. Rev. Lett. **81**, 5048 (1998).
[39] A. R. Bulsara, V. In, A. Kho, P. Longhini, A. Palacios, W.-J. Rappel, J. Acebron, S. Baglio, and B. Ando, Phys. Rev. E **70**, 036103 (2004).
[40] M. Perc, Phys. Rev. E **76**, 066203 (2007).
[41] F. Lu and Z. Liu, Chin. Phys. Lett. **26**, 040503 (2009).
[42] D. J. Watts and S. H. Strogatz, Nature (London) **393**, 440 (1998).
[43] A.-L. Barabási and R. Albert, Science **286**, 509 (1999).
[44] S. H. Strogatz, *Nonlinear Dynamics and Chaos: With Applications to Physics, Biology, Chemistry, and Engineering* (Westview Press, Boulder, CO, 2015).
[45] Y. Lei and F. Guan, Int. J. Mod. Phys. C **23**, 1250071 (2012).
[46] R. Benzi, A. Sutera, and A. Vulpiani, J. Phys. A: Math. Gen. **14**, L453 (1981).
[47] V. S. Anishchenko, A. N. Silchenko, and I. A. Khovanov, Phys. Rev. E **57**, 316 (1998).
[48] K. V. Mardia and P. E. Jupp, *Directional Statistics*, 2nd ed. Wiley Series in Probability and Statistics (Wiley, Chichester, 2000).
[49] J. J. Collins, C. C. Chow, and T. T. Imhoff, Phys. Rev. E **52**, R3321 (1995).
[50] Z. Liu, Y. Lai, and A. Nachman, Int. J. Bifurcation Chaos **14**, 1655 (2004).
[51] X. Liang, L. Zhao, and Z. Liu, Phys. Rev. E **84**, 031916 (2011).
[52] P. J. Martínez and R. Chacón, Phys. Rev. E **93**, 042311 (2016).
[53] R. Chacón, F. Palmero, and J. Cuevas-Maraver, Phys. Rev. E **93**, 062210 (2016).